

## Irreversible critical current and the anomalous magnetic-moment peak in silver-sheathed (Pb,Bi)<sub>2</sub>Sr<sub>2</sub>Ca<sub>2</sub>Cu<sub>3</sub>O<sub>10+y</sub> tapes

K.-H. Müller and C. Andrikidis

*Commonwealth Scientific and Industrial Research Organization, Division of Telecommunication and Industrial Physics, Lindfield, Australia 2070*

Y. C. Guo

*Centre for Superconducting and Electronic Materials, University of Wollongong, Australia 2522*

(Received 1 May 1996; revised manuscript received 12 September 1996)

We have measured under zero-field-cooled (ZFC) and field-cooled (FC) conditions the magnetic moments of a high-quality (Pb,Bi)<sub>2</sub>Sr<sub>2</sub>Ca<sub>2</sub>Cu<sub>3</sub>O<sub>10+y</sub> tape at 5 K in perpendicular applied fields up to 1 T using a superconducting quantum interference device magnetometer. The intergranular magnetic moment, obtained by subtracting from the total magnetic moment the intragranular moment of the ‘bent’ tape shows a pronounced anomalous peak at a positive field  $H_p$ . To interpret the experimental data the critical-state model for a flat superconducting strip in a perpendicular field is employed. The model includes the field dependence of the intergranular critical current density in first order. The field at grain-boundary Josephson junctions, which strongly influences the intergranular current, is estimated by taking the demagnetizing effect of the grains into account. The model predicts correctly the measured intergranular magnetic moments and the behavior of the anomalous peak in both the ZFC and the FC case. The saturation of the remanent intragranular magnetization occurs at a lower maximum field than the saturation of  $H_p$  which can be well understood in terms of the demagnetizing effect of the grains. A model which neglects grain demagnetization but instead takes the vortex distribution of vortices near Josephson junctions into account cannot describe quantitatively the observed behavior of the anomalous peak. [S0163-1829(97)02701-X]

### I. INTRODUCTION

Silver-sheathed (Pb,Bi)<sub>2</sub>Sr<sub>2</sub>Ca<sub>2</sub>Cu<sub>3</sub>O<sub>10+y</sub> tapes (PBSCCO tapes) consist of thin, about 10  $\mu\text{m}$  wide grain platelets where the platelets generally align within  $5^\circ$ – $10^\circ$  with the  $c$  direction perpendicular to the plane of the tape and the  $a$  and  $b$  directions are oriented at random from platelet to platelet.<sup>1</sup> This grain alignment in conjunction with a high density gives the tape a very high intergranular (transport) critical current density  $J_{cJ}$ . Measuring the magnetic moment of a tape, one finds that it consists of two parts, the intergranular moment, originating from an induced intergranular (transport) current and the intragranular magnetic moment, originating from induced currents circulating in grains.<sup>2,3</sup> In most PBSCCO tapes the intergranular magnetic moment is greater than the intragranular one simply because of the large intergranular critical current density  $J_{cJ}$ . This is contrary to non-grain-aligned polycrystalline high-temperature superconductors where, because of the small intergranular critical current density in these materials, the intergranular moment is much weaker than the intragranular one. As in non-grain-aligned polycrystalline high-temperature superconductors,<sup>4–9</sup> the transport critical current of PBSCCO tapes shows hysteretic behavior<sup>10</sup> which is attributed to the presence of trapped flux in the grains. Using the electrical four-point-probe method one finds that, because of the grain-boundary weak links, the critical current density decreases rapidly in an increasing applied field.<sup>11</sup> In the zero-field-cooling (ZFC) case, if one stops the field sweep at a maximum field  $H_m$  which is greater than  $H_{c1G}$  (lower critical field of the grains) and then decreases the applied field, one finds  $J_{cJ}$  to be greater than the initial, virgin critical current density and  $J_{cJ}$  goes through

a maximum at a positive field  $H_p$ .<sup>4–10</sup> In the field-cooling (FC) case one finds a similar behavior for  $J_{cJ}$  but now  $H_{p,FC} \geq H_{p,ZFC}$  because of the different amounts of flux trapped under FC and ZFC conditions.<sup>7</sup> The hysteretic behavior of  $J_{cJ}$  is most pronounced at low temperature. Because  $J_{cJ}$  is large in the PBSCCO tapes, the hysteretic behavior of  $J_{cJ}$  has a strong effect on the shape of the magnetic moment  $m$ . In good tapes, where the intergranular magnetic moment is larger than the intragranular one, a pronounced anomalous peak appears at a positive applied field which, according to the critical-state model, corresponds to the peak behavior of  $J_{cJ}$ .<sup>2,12–14</sup>

Evetts and Glowacki<sup>4</sup> have interpreted the hysteretic behavior of  $J_{cJ}$  in the ZFC case in a qualitative way by applying the critical-state model to the grains, arguing that the resulting dipole field of the grains, which spills into the intergranular region, causes the observed hysteresis. Quite a different model has been proposed by D'yachenko<sup>9</sup> in which the hysteretic behavior of  $J_{cJ}$  is assumed to be caused by the change in the direction of the intragranular current near the grain surface where the current adds to—or subtracts from—the Meissner shielding current, depending on whether the applied field is being increased or decreased.

We employ a simple theoretical model whose main features were initially proposed by Zhukov *et al.*<sup>6</sup> It strongly relates to the idea of the qualitative Evetts model which has been extended to explain quantitatively the hysteretic behavior of  $J_{cJ}$  in non-grain-aligned polycrystalline high-temperature superconductors.<sup>7,8</sup> The model used in this paper is based on the demagnetizing effect of the grains which affects the magnetic field that threads the grain-boundary Josephson junction. In the model the demagnetization depends

on the irreversible magnetization of the grains which in turn causes the critical current density to become irreversible resulting in the appearance of an anomalous peak in the intergranular magnetic moment.

In Sec. II we briefly describe the experiment to measure the intergranular and intragranular magnetic moments as a function of a magnetic field, applied perpendicular to the tape. In Sec. III we discuss the equations which describe the intergranular magnetic moment of the PBSCCO tape in a perpendicular magnetic field and introduce the demagnetizing effect of grains into the model. In Sec. IV we compare the experimental data of the intergranular magnetic moment with the predictions of our theoretical model and elucidate the dependence of the anomalous peak on the maximum applied field for both ZFC and FC conditions. We demonstrate that the demagnetizing effect of the grains is responsible for the observed behavior of the anomalous peak seen in the intergranular magnetic moment of PBSCCO tapes and we show that the D'yachenko model<sup>9</sup> cannot describe quantitatively the behavior of the anomalous peak.

Finally in Sec. V we summarize our findings. In the Appendix we derive equations for the anomalous peak using the D'yachenko model.

## II. EXPERIMENT

The monofilamentary tape, used in our measurements, was prepared by employing the powder-in-tube method where strong alignment of the grains is achieved by pressing and rolling of the PBSCCO powder encapsulated in a silver sheath. Details about this method have been reported in Ref. 15. X-ray-diffraction measurements indicated that the core of the tape consisted of almost pure 2223 phase with only very small amounts of 2212 phase present. Using a four-point-probe method, with the usual  $1 \mu\text{V}/\text{cm}$  electric-field criterion, the transport critical current density was found to be  $16\,000 \text{ A}/\text{cm}^2$  at  $77 \text{ K}$  in zero applied field. The average thickness of the superconducting core was  $60 \mu\text{m}$  and the width of the core was about  $2.3 \text{ mm}$ . Two pieces of equal length of  $5.8 \text{ mm}$  were cut from a longer tape. The second piece was severely curled (bent) along its rolling direction to the small diameter of  $\sim 1.2 \text{ mm}$  and finally straightened. A commercial Quantum Design superconducting quantum interference device (SQUID) magnetometer was employed to measure the magnetic moments of the two pieces of the tape, the "intact" tape and the "bent" one, at  $5 \text{ K}$  under both zero-field-cooled (ZFC) and field-cooled (FC) conditions. The field was applied perpendicular to the tape surface, i.e., parallel to the crystallographic  $c$  direction of the grains. A 5-cm scan was used and the magnetic field was swept in the no-overshoot mode from the maximum field  $H_m$  to  $-H_m$  with  $\mu_0 H_m$  between  $25 \text{ mT}$  and  $1 \text{ T}$ .

## III. THEORETICAL MODEL

A PBSCCO tape can be viewed as a grain network where the grains are well linked by grain-boundary Josephson junctions. The current density,  $\mathbf{J}(\mathbf{r})$  at point  $\mathbf{r}$  inside the tape can be split into two parts, the intergranular current density  $\mathbf{J}_J(\mathbf{r})$  and the intragranular current density  $\mathbf{J}_G(\mathbf{r})$  where

$$\mathbf{J}(\mathbf{r}) = \mathbf{J}_J(\mathbf{r}) + \mathbf{J}_G(\mathbf{r}). \quad (1)$$

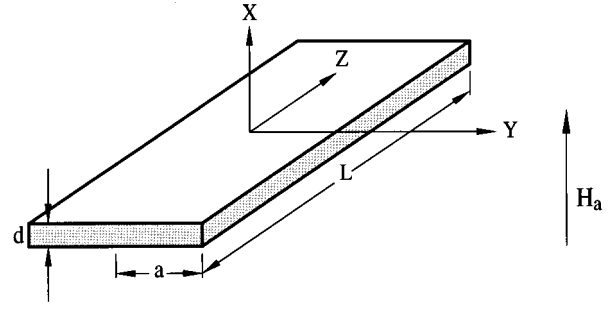


FIG. 1. Superconducting core of the monofilamentary tape approximated by a thin superconducting strip of thickness  $d$ , half width  $a$ , and length  $L$ .

The intergranular current is the Josephson current (thus the subscript  $J$ ) flowing across grain boundaries while the intragranular current is flowing inside grains (thus the subscript  $G$ ) and is determined by the pinning of pancake vortices in the grains.<sup>2,16</sup> By averaging the microscopic intergranular current density  $\mathbf{J}_J(\mathbf{r})$  over a volume large compared to the grain size but small compared to the dimensions of the tape, one obtains the transport current density  $\langle \mathbf{J}_J \rangle(\mathbf{r})$  which flows over the entire tape.

It has been shown by Majhofer and co-workers<sup>17,18</sup> that the critical current  $J_{cJ}$  of a Josephson network is determined not only by the magnitude of the Josephson critical current but also by the inductances of the Josephson-junction loops, formed by adjacent grains. Majhofer and co-workers<sup>17,18</sup> also showed that the magnetic-field behavior of the Josephson network can be described in terms of a critical-state model where the magnetic field penetrates the sample in a "Bean-like" fashion. Tinkham and Lobb<sup>19</sup> demonstrated that besides intrinsic pinning, which is inherent to a Josephson array, disorder, and defect pinning are of importance.

The transport current density distribution  $\langle J_J \rangle$  which is induced in a superconducting strip (or tape), where the magnetic field  $H_a$  is applied perpendicular to the strip, has been calculated by Brandt and Indenbom<sup>20</sup> and later by Zeldov *et al.*<sup>21</sup>

In the zero-field-cooled case (ZFC), the induced transport current density  $\langle J_{J1} \rangle$  which is flowing along the positive and negative  $z$  direction (see Fig. 1) when the applied field  $H_a$  is decreased ( $\downarrow$ ) from the maximum applied field  $H_m$  to  $H_a$ , is given by

$$\langle J_{J1} \rangle(y, \text{ZFC}) = \langle J_J \rangle(y, H_m, J_{cJ}) - \langle J_J \rangle(y, H_m - H_a, 2J_{cJ}), \quad (2)$$

where

$$\langle J_J \rangle(y, H_a, J_{cJ}) = \begin{cases} \frac{2J_{cJ}}{\pi} \arctan \frac{cy}{\sqrt{b^2 - y^2}}; & |y| \leq b \\ J_{cJ}; & b < |y| < a \end{cases} \quad (3)$$

with

$$c = \frac{\sqrt{a^2 - b^2}}{a}, \quad b = \frac{a}{\cosh(H_a/H_d)} \quad \text{and} \quad H_d = J_{cJ}d/\pi. \quad (4)$$

Here,  $a$  is the half width and  $d$  is the thickness of the tape as indicated in Fig. 1.  $J_{cJ}$  is the field-independent intergranular critical current density where  $|\langle J_J \rangle(y)| \leq J_{cJ}$ .

In the field-cooled case (FC) we find

$$\langle J_{J\downarrow} \rangle(y, \text{FC}) = -\langle J_J \rangle(y, H_m - H_a, J_{cJ}). \quad (5)$$

Notice that here the last argument of  $\langle J_J \rangle$  is  $J_{cJ}$  and not  $2J_{cJ}$  as in Eq. (2). From the current density distribution  $\langle J_{J\downarrow} \rangle(y)$  the intergranular magnetic field  $H_{J\downarrow}(y)$  in  $x$  direction can be calculated using Biot-Savart's law. To an accuracy of  $d/a$  one finds<sup>20</sup>

$$H_{J\downarrow}(y) = \frac{d}{2\pi} \int_{-a}^a \frac{\langle J_{J\downarrow} \rangle(u) du}{y-u} + H_a. \quad (6)$$

When the applied field is decreased from  $H_m$  to  $H_a$  one obtains for the ZFC case

$$H_{J\downarrow}(y, \text{ZFC}) = H_J(y, H_m, J_{cJ}) - H_J(y, H_m - H_a, 2J_{cJ}), \quad (7)$$

where

$$H_J(y) = \begin{cases} 0; & |y| \leq b \\ H_d \operatorname{arctanh} \frac{\sqrt{y^2 - b^2}}{c|y|}; & b < |y| < a \\ H_d \operatorname{arctanh} \frac{c|y|}{\sqrt{y^2 - b^2}}; & |y| < a. \end{cases} \quad (8)$$

And in the FC case we obtain

$$H_{J\downarrow}(y, \text{FC}) = H_m - H_J(y, H_m - H_a, J_{cJ}). \quad (9)$$

Notice that the second term on the right contains  $J_{cJ}$  and not  $2J_{cJ}$  like the second term in Eq. (7).

To derive the above analytical expressions for  $\langle J_{J\downarrow} \rangle$  it was assumed that  $J_{cJ}$  is independent of the magnetic field  $H_{J\downarrow}$  inside the superconductor. This is an oversimplifying assumption, as the transport current of a Josephson network generally decreases monotonically in an increasing magnetic field. By taking the field dependence of the current density into account one obtains an improved description of the magnetic properties of the Bi-2223 tape, as we shall see below. It is of great importance to notice that the field at a grain-boundary Josephson junction does not only depend on the intergranular magnetic field  $H_{J\downarrow}$ , but also on the magnetic field generated by the grains adjacent to that junction.<sup>4,6-8</sup> Therefore, in addition to the intergranular magnetic field, field lines originating from grains thread the junction. The main idea of this paper is that the field  $H_i$  at a grain boundary can be approximated by

$$H_i = H_{J\downarrow} - \Gamma M_G(H_i, H_{im}), \quad (10)$$

which is an implicit equation for  $H_i$ , where the second term on the right is the contribution to the magnetic field from the grains. Here,  $\Gamma$  is the average demagnetizing factor of the grain network and  $M_G$  the average grain magnetization. The field  $H_{im}$  is the maximum field that was present at a grain boundary before the applied field was decreased and  $H_{im}$  is defined by the equation

$$H_{im} = H_{J\downarrow}(H_a = H_m) - \Gamma M_G(H_{im}, H_{im}). \quad (11)$$

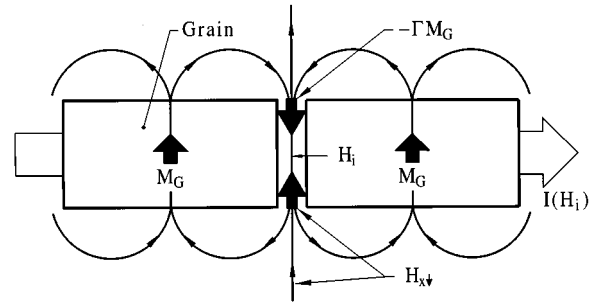


FIG. 2. Schematic of magnetic fields at a grain boundary.

Because the grain magnetization  $M_G$  is irreversible,  $H_i$  is hysteretic and thus the transport current of the tape, which is determined by Josephson currents, shows hysteretic behavior. The essence of the above described model is illustrated in Fig. 2 which shows schematically two grains where the intergranular current  $I(H_i)$  crosses the grain boundary. The field  $H_i$  between the grains is composed of the intergranular field  $H_{x\downarrow}(y)$  and the return-field,  $-\Gamma M_G$ , of the grains.

Equation (10) is an exact expression for a homogeneously magnetized, isolated ellipsoid in an external field of size  $H_{J\downarrow}$  where the field  $H_i$  is the magnetic field inside the ellipsoid with the tangential component of  $H_i$  being steady at the surface.<sup>22</sup> The case of two spherical grains close together has been discussed by Waysand,<sup>23</sup> while more complicated configurations of grains have been investigated by Hodgdon, Navarro, and Campbell,<sup>24</sup> where in addition comparisons with the effective mean-field theory were made. An attempt to estimate  $\Gamma$ , using the magnetic dipole approximation, has been made by Altshuler.<sup>8</sup> In reality the demagnetization factor will vary from one grain boundary to the next and thus the factor  $\Gamma$  in Eq. (10) is meant to be an average of the demagnetizing factors of the grain network.

To correct in first order for the missing field dependence of  $J_{cJ}$ , we introduce the revised current density  $\langle \tilde{J}_{J\downarrow} \rangle$  to calculate the intergranular magnetic moment  $m_{J\downarrow}$  where

$$\langle \tilde{J}_{J\downarrow} \rangle = \langle J_{J\downarrow} \rangle \frac{H_0^n}{(H_0 + |H_i|)^n}. \quad (12)$$

Notice that  $\langle \tilde{J}_{J\downarrow} \rangle$  depends on  $H_i$  and not on  $H_{J\downarrow}$  which accounts for the demagnetizing effect of grains and that  $H_{J\downarrow}$  in Eq. (10) is calculated using  $\langle J_{J\downarrow} \rangle$  and not  $\langle \tilde{J}_{J\downarrow} \rangle$  which makes it a first-order correction scheme to include the field dependence of the intergranular critical current density into the model. The exponent  $n$  and the field  $H_0$  depend on the type of Josephson junctions<sup>25</sup> and the morphology of the network<sup>18,19</sup> and both  $n$  and  $H_0$  are treated here as phenomenological parameters.

For the grain magnetization  $M_G$  we adopted the simple expressions derived from the Bean model<sup>26,27</sup> for an infinite slab of thickness  $2R_G$ , where  $R_G$  corresponds to the average grain radius, in a parallel field. The Bean model assumes that the critical current density of grains,  $J_{cG}$ , is field independent and  $H_{c1G} = 0$ . One finds for decreasing  $H_i$  in the ZFC case

$$M_G^{\text{ZFC}} = \begin{cases} \frac{H_{im}^2}{2H^*} - \frac{(H_i - H_{im})^2}{4H^*} - H_i; & H_{im} < H^* \\ H_{im} - \frac{H^*}{2} - \frac{(H_i - H_{im})^2}{4H^*} - H_i; & H_{im} - 2H^* \leq H_i \\ \frac{H^*}{2}; & H_i < H_{im} - 2H^*. \end{cases} \quad (13)$$

Here,  $H^*$  is the field of full penetration into grains, i.e.,  $H^* = J_{cG}R_G$ .

In the FC case one finds<sup>28</sup>

$$M_G^{\text{FC}} = \begin{cases} H_{im} - H_i - \frac{(H_{im} - H_i)^2}{2H^*} - H_i; & H_{im} - H_i \leq H^* \\ \frac{H^*}{2}; & H_{im} - H_i > H^*. \end{cases} \quad (14)$$

Figures 3(a) and 3(b) show a schematic drawing of  $H_i$  versus  $H_{J\perp}$  for the ZFC and FC cases, respectively, using Eq. (10). As can be seen, when  $H_{J\perp}$  decreases, the field  $H_i$  becomes zero at  $H_{J\perp} = H_p > 0$  where  $H_{p,\text{ZFC}} \approx H_{p,\text{FC}}$ . According to Eq. (12), the transport current  $\langle J_{J\perp} \rangle$  reaches its maximum at  $H_p$ .

Figure 4 shows the field distributions  $H_{J\perp}$  and  $H_i$  as a function of  $y$  across the superconducting tape. Because the applied field is perpendicular to the surface of the tape, the field near the edges reaches values greater than  $H_m$ . The values for  $H_i$  can differ significantly from  $H_{J\perp}$ , indicating the importance of the grain demagnetizing effect.

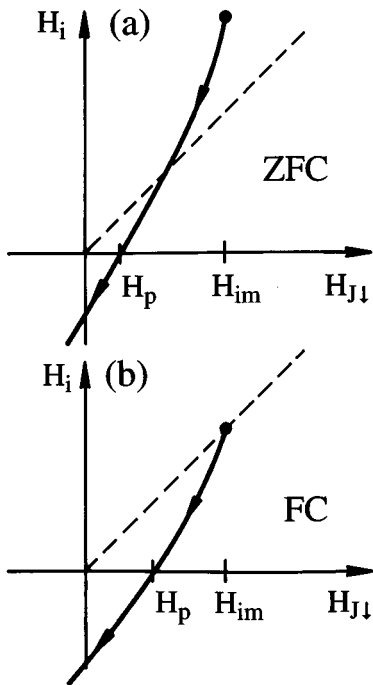


FIG. 3. Schematic of the field  $H_i$  at a grain boundary due to the demagnetizing effect of adjacent grains as a function of the decreasing intergranular magnetic field  $H_{J\perp}$  for (a) ZFC condition and (b) FC condition.  $H_{im}$  is the maximum field at a grain boundary.

The total magnetic moment  $\mathbf{m}$  is defined as

$$\mathbf{m} = \frac{1}{2} \int \mathbf{r} \times \mathbf{J}(\mathbf{r}) d^3r. \quad (15)$$

For a superconducting tape in perpendicular field  $H_a$ , where  $H_a$  was set by decreasing the applied field from  $H_m$  to  $H_a$ , one obtains for the intergranular magnetic moment<sup>20,2</sup>

$$m_{J\perp} = 2Ld \int_0^a y \tilde{J}_{J\perp}(y) dy. \quad (16)$$

The magnetic field  $H_p$ , where the intergranular magnetic moment  $m_J$  peaks, as a function of the maximum applied field  $H_m$ , can be determined from calculations of the magnetic-moment loops  $m_J(H_a, H_m)$ .

Instead of doing a lengthy calculation for  $H_p$  using Eqs. (2)–(16), one can get an approximate value for  $H_p$  in the case of  $H_m \gg H_d$  by using Eq. (10) with  $H_i = 0$  and  $H_{J\perp} = H_p$  which results in

$$H_p \approx \Gamma M_G[H_i = 0, H_{im}(H_m)]. \quad (17)$$

Because  $M_G$  saturates at large  $H_m$ , the peak field  $H_p$  also saturates and it is thus useful to compare the saturation of  $H_p$  with the saturation of the remanent intragranular magnetization  $M_G^R$  of the grains. The remanent intragranular magnetization  $M_G^R$  is defined by Eq. (10) for  $H_{J\perp} = 0$  which gives

$$H_i^R = -\Gamma M_G(H_i^R, H_{im}). \quad (18)$$

Thus

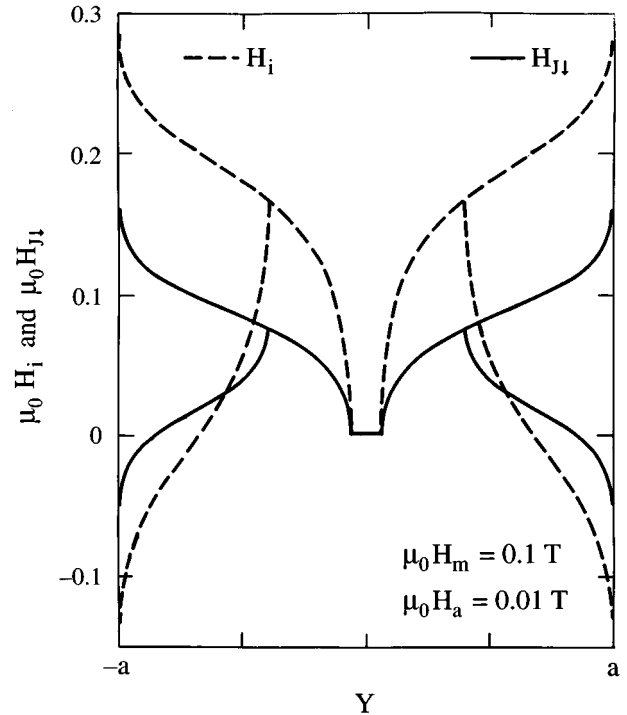


FIG. 4. Calculated intergranular magnetic field  $H_{J\perp}$  and magnetic field  $H_i$  at grain boundaries as a function of the position  $y$  along the width of the superconducting core of the tape for a maximum field of  $\mu_0 H_m = 0.1$  T and an applied field  $\mu_0 H_a = 0.01$  T.

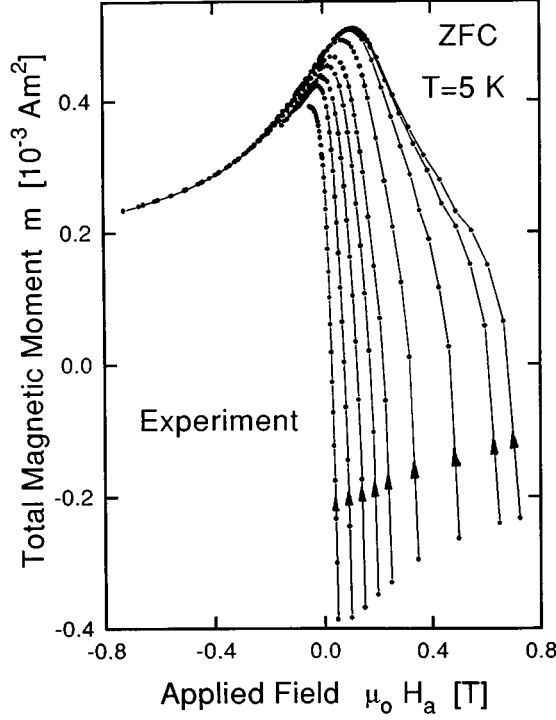


FIG. 5. Measured total magnetic moment  $m_{\perp}$  (intact tape) under ZFC conditions at 5 K versus the applied magnetic field  $H_a$  for different maximum fields  $H_m$ . The applied field, after an initial increase from 0 to  $H_m$ , is decreased from  $H_m$  to  $-H_m$ .

$$M_G^R \equiv M_G(H_i^R, H_{im}). \quad (19)$$

Notice that when measuring the intragranular magnetization no intergranular current is present and  $H_{J\perp} = H_a$ . In the limit of  $\Gamma \rightarrow 0$ , both  $H_p$  and  $M_G^R$  saturate in the same fashion which will be illustrated later in Figs. 16 and 17.

The model described above [Eqs. (10)–(14)] is essentially a mathematical formulation of the qualitative Evetts model.<sup>4</sup> Our model goes beyond the Evetts model as it takes into account the effect of the magnetic field which is generated by the intergranular current. While in this work the anomalous peak in the magnetic moment of a PBSCCO tape is investigated, Evetts and Glowacki<sup>4</sup> measured the irreversible critical current density as a function of the applied field using the electrical four-point-probe method. This irreversible critical current density is given by Eq. (12) with  $\langle J_{J\perp} \rangle = J_c$ . A model for the irreversible critical current based on Eqs. (10) and (12) has been reported in Ref. 7.

#### IV. RESULTS AND DISCUSSION

Figure 5 shows the measured ZFC total magnetic moment  $m_{\perp}$  of the “intact” tape at 5 K for a decreasing applied field  $H_a$  where the maximum applied fields are  $\mu_0 H_m = 0.05, 0.1, 0.15, 0.2, 0.25, 0.35, 0.5, 0.65,$  and  $0.725$  T. The magnetic moment  $m_{\perp}$  for an increasing applied field is simply given by  $m_{\perp}(H_a, H_m) = -m_{\perp}(-H_a, H_m)$  and is therefore not shown. The most striking feature of Fig. 5 is the anomalous peak positioned at a positive applied field while commonly superconductors show a peak in the magnetic moment at a nega-

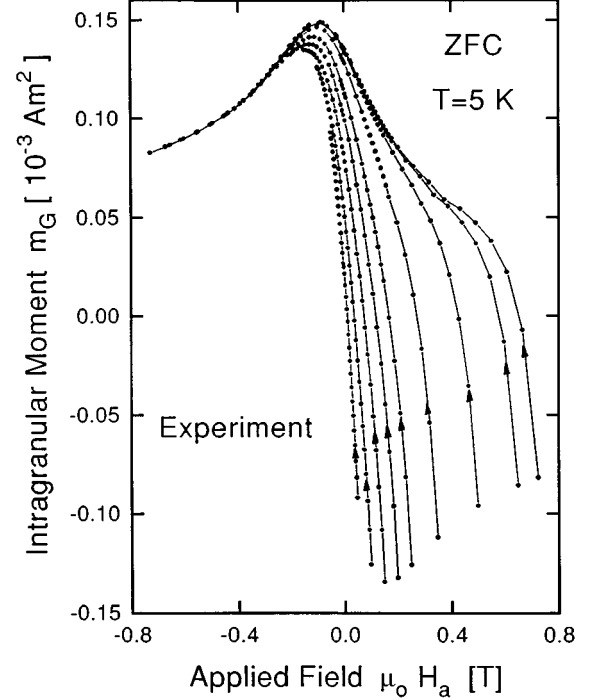


FIG. 6. Measured intragranular magnetic moment  $m_{G\perp}$  (bent tape) under ZFC conditions at 5 K versus the applied magnetic field  $H_a$  for different maximum fields  $H_m$ . The applied field, after an initial increase from 0 to  $H_m$ , is decreased from  $H_m$  to  $-H_m$ .

tive applied field. The virgin part of the magnetic moment is not shown for clarity.

Figure 6 shows the measured ZFC intragranular magnetic moment  $m_{G\perp}$  of the “bent” tape for different values of  $H_m$ . The intragranular magnetization shows, as expected, a peak at a negative applied field which shifts slightly to less negative fields with increasing maximum field  $H_m$ . The origin of this intragranular peak is well understood in terms of a critical state model in which the intragranular critical current density is field dependent and decreases monotonically with increasing field. Figure 6 reveals that roughly 25% of the total magnetic moment originates from currents induced in the grains. The question that arises here is whether the so-called intragranular magnetic moment is indeed only been caused by currents flowing in grains and not by currents flowing in larger grain clusters. To answer this question we have studied in Ref. 2 the remanent magnetic moment of the tape as a function of the degree of bending and in Ref. 13 we crushed the tape and carefully scraped the core material out of the silver cladding and measured its magnetic moment. The investigations revealed that the magnetic moment of a strongly bent tape is that of the grains and that the contribution from grain clusters, in which the intergranular current is flowing, is negligibly small.

Figure 7 displays the measured intergranular ZFC magnetic moment  $m_{J\perp}$ , obtained by subtracting from the data of Fig. 5 the data of Fig. 6 where  $m_{J\perp} = m_{\perp} - m_{G\perp}$ . The anomalous peak is even more pronounced than in the case of the intact tape. The inset in Fig. 7 shows more clearly the evolution of the anomalous peak as a function of the maximum field  $H_m$ .

The calculated intergranular ZFC magnetic moment  $m_{J\perp}$ ,

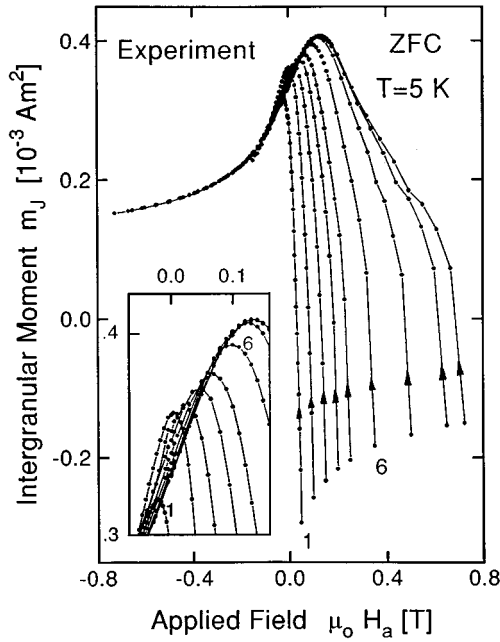


FIG. 7. Measured intergranular magnetic moment  $m_{J\perp}$  under ZFC conditions at 5 K versus the applied magnetic field  $H_a$  for different maximum fields  $H_m$ . The applied field, after an initial increase from 0 to  $H_m$ , is decreased from  $H_m$  to  $-H_m$ . The inset shows the evolution of the anomalous peak for different maximum fields  $H_m$ .

using the model developed in this paper [Eqs. (2)–(16)], is displayed in Fig. 8. The parameters used are  $d=60 \mu\text{m}$ ,  $a=1.1 \text{ mm}$ ,  $n=2$ ,  $\mu_0 H_0=1 \text{ T}$ ,  $J_c=1.2 \times 10^9 \text{ A m}^{-2}$ ,  $\mu_0 H^*=0.38 \text{ T}$ , and  $\Gamma=0.7$ . The calculated moment  $m_{J\perp}$

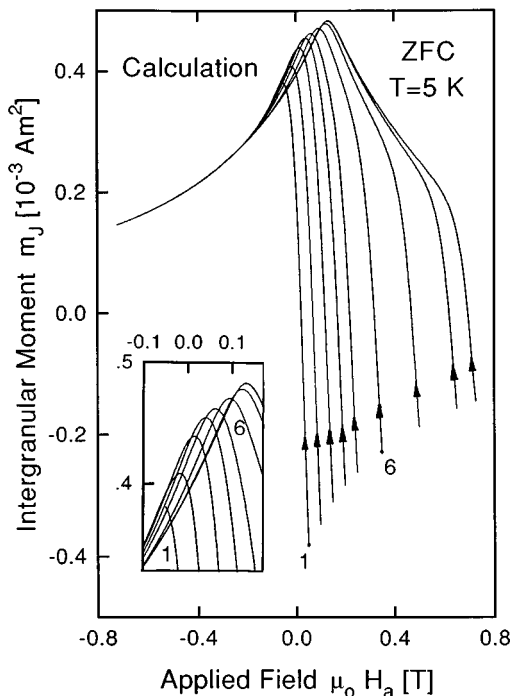


FIG. 8. Calculated intergranular magnetic moment  $m_{J\perp}$  under ZFC conditions at 5 K versus the applied magnetic field  $H_a$  for different maximum fields  $H_m$ . The inset shows the evolution of the anomalous peak for different maximum applied fields  $H_m$ .

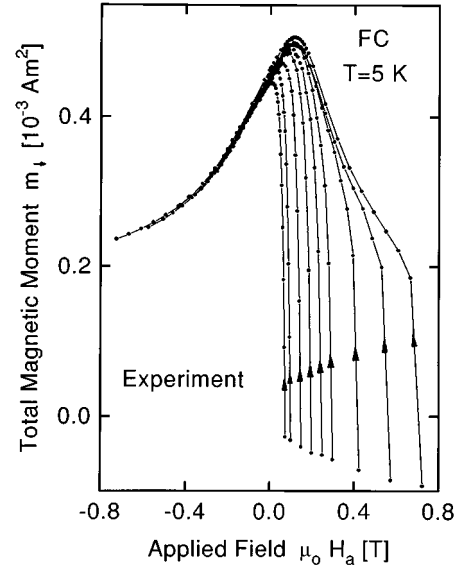


FIG. 9. Measured total magnetic moment  $m_{\perp}$  (intact tape) under FC conditions at 5 K versus the applied magnetic field  $H_a$  for different maximum fields  $H_m$ . The applied field is decreased from  $H_m$  to  $-H_m$ .

shows excellent resemblance with the experimental data of Fig. 7 and the evolution of the anomalous peak for increasing  $H_m$  is well reproduced.

Figure 9 shows the measured FC total magnetic moment  $m_{\perp}$  of the intact tape at 5 K for a decreasing applied field  $H_a$  at  $\mu_0 H_m=0.075, 0.1, 0.15, 0.2, 0.25, 0.3, 0.425, 0.575$ , and  $0.725 \text{ T}$ . The FC magnetic moment  $m_{J\perp}$  at  $H_a=H_m$  has a value close to zero which is different to the ZFC case in Fig. 5 as more flux penetrates the sample at  $H_a=H_m$  in the FC case than in the ZFC one. Like under the ZFC condition, an anomalous peak appears at a positive field.

Figure 10 shows the measured intragranular magnetic moment  $m_{G\perp}$  of the bent tape. Like in the ZFC case, the peak in the intragranular magnetic moment appears at negative applied fields. There is a clear difference between the magnitudes of the ZFC and the FC intragranular magnetic moments at  $H_a=H_m$ . Figure 10 reveals that roughly 25% of the total magnetic moment originates from currents induced in the grains.

Figure 11 displays the measured intergranular FC magnetic moment  $m_{J\perp}$  where  $m_{J\perp}=m_{\perp}-m_{G\perp}$ . The inset shows the anomalous peak for different  $H_m$  in greater detail.

Figure 12 shows the calculated intergranular FC magnetic moment  $m_{J\perp}$  using the model developed in this paper [Eqs. (2)–(16)]. The parameters used are the ones used to calculate the ZFC intergranular magnetic moment in Fig. 8. There is a strong resemblance to the experimental data of Fig. 11 and, as indicated in the inset, the evolution of the anomalous peak for increasing  $H_m$  is reasonably well reproduced.

Figure 13 compares the measured  $H_p(H_m)$  data with the measured intragranular remanent magnetic moment  $m_G^R(H_m)=m_{G\perp}(H_a=0, H_m)$  for the ZFC case, respectively. The remanent intragranular magnetic moment  $m_G^R$  saturates before saturation of  $H_p$  occurs and both curves are shifted with respect to the  $H_m$  axis by about 0.1 T.

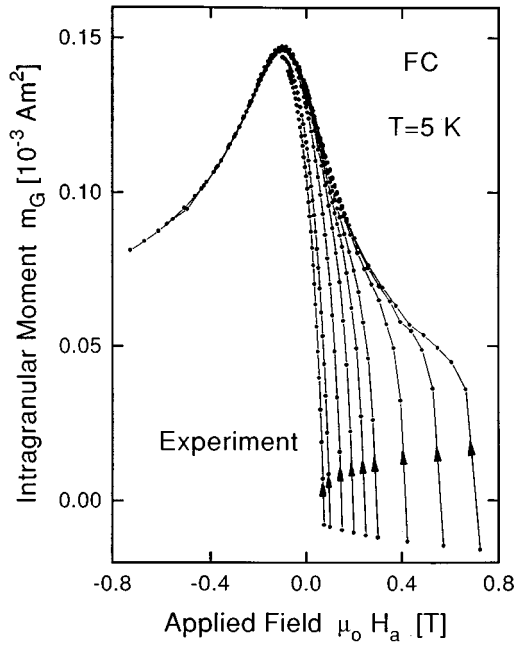


FIG. 10. Measured intragranular magnetic moment  $m_{G\downarrow}$  (bent tape) under FC conditions at 5 K versus the applied magnetic field  $H_a$  for different maximum fields  $H_m$ . The applied field is decreased from  $H_m$  to  $-H_m$ .

Figure 14 shows the calculated values of  $H_p$  and  $m_G^R$  versus  $H_m$  which agrees reasonably well with the experimental data of Fig. 13. The anomalous peak field  $H_p$  was calculated by using Eqs. (2)–(16) and  $H_p$  was determined numerically by calculating where  $m_{J\downarrow}$  peaks. To calculate  $m_G^R$  Eqs.

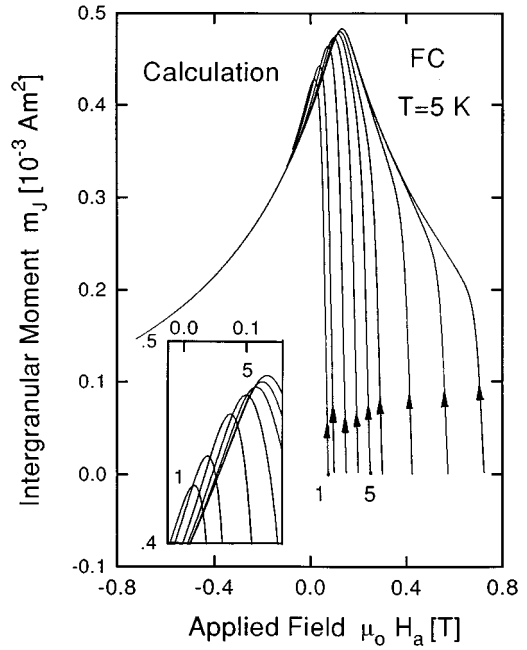


FIG. 12. Calculated intergranular magnetic moment  $m_{J\downarrow}$  under FC conditions at 5 K versus the applied magnetic field  $H_a$  for different maximum fields  $H_m$ . The inset shows the evolution of the anomalous peak for different maximum applied fields  $H_m$ .

(18) and (19) with  $\Gamma=0.7$  were used, where  $m_G^R = 2adLM_G^R$ .

Figures 15 and 16 display experimental data and calculations of  $H_p$  and  $m_G^R$  versus  $H_m$  in the FC case. As can be seen, in the FC case,  $H_p$  saturates at about  $\mu_0 H_m = 0.4$  T,

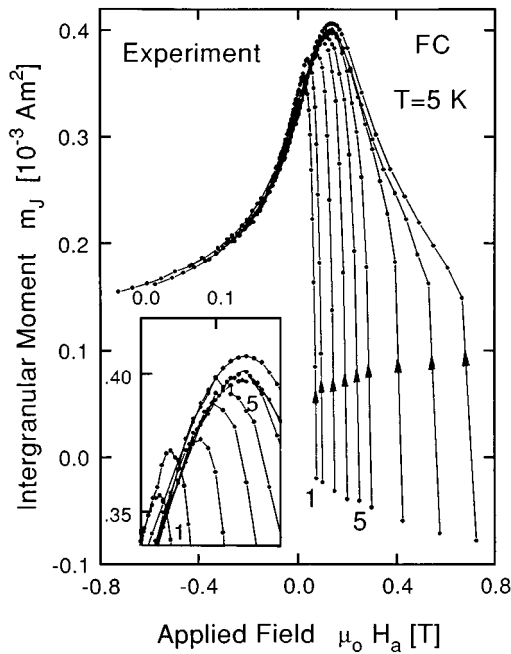


FIG. 11. Measured intergranular magnetic moment  $m_{J\downarrow}$  under FC conditions at 5 K versus the applied magnetic field  $H_a$  for different maximum fields  $H_m$ . The applied field is decreased from  $H_m$  to  $-H_m$ . The inset shows the evolution of the anomalous peak for different maximum applied fields  $H_m$ .

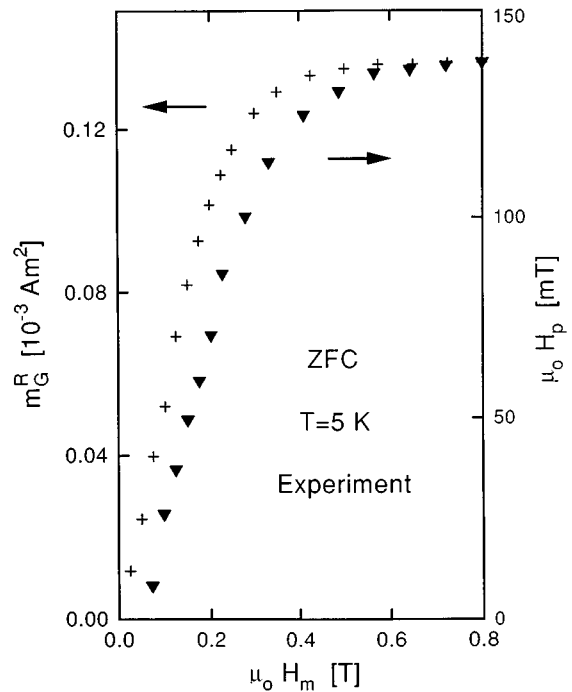


FIG. 13. Measured intragranular remanent magnetic moment  $m_G^R$  and the measured anomalous peak field  $H_p$  at 5 K under ZFC conditions as a function of the maximum applied field  $H_m$ .

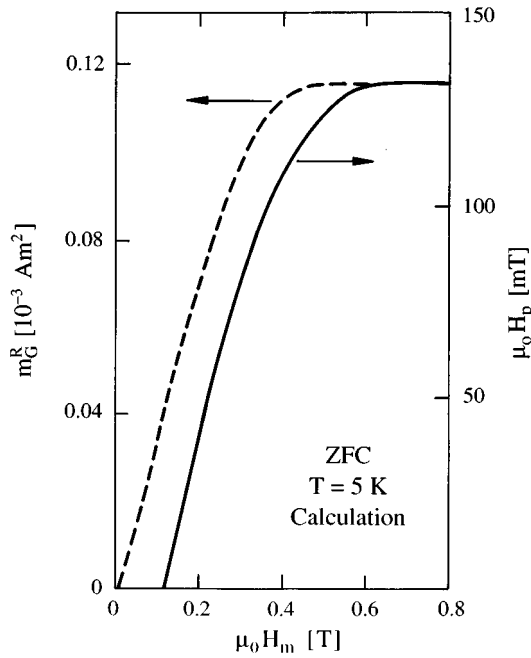


FIG. 14. Calculated intergranular remanent magnetic moment  $m_G^R$  and the calculated anomalous peak field  $H_p$  at 5 K under ZFC conditions as a function of the maximum applied field  $H_m$ .

while in the ZFC case (Fig. 13),  $H_p$  saturates at about  $\mu_0 H_m = 0.6$  T.

Figures 17 and 18 show the calculated ZFC and FC remanent magnetization  $M_G^R(H_m)$  as defined by Eqs. (18) and (19) and the peak field  $H_p(H_m)$  approximated by Eq. (17) for  $\Gamma=1/3$  and  $\Gamma=1$ . The difference in the saturation of  $M_G^R$  (or

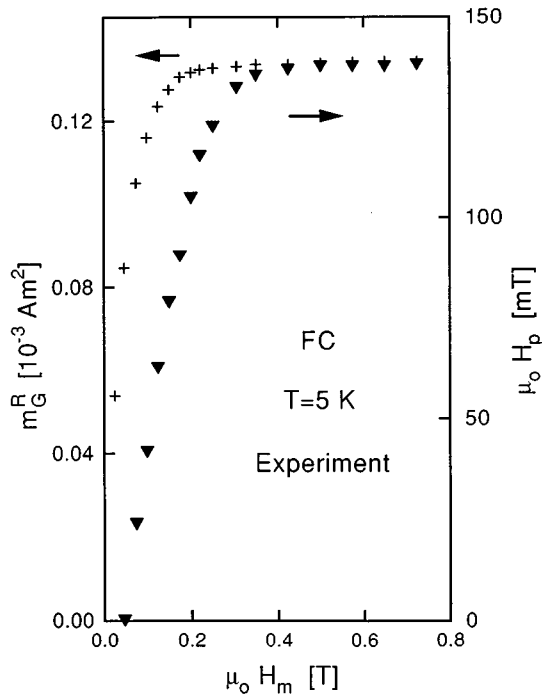


FIG. 15. Measured intragranular remanent magnetic moment  $m_G^R$  and the measured anomalous peak field  $H_p$  at 5 K under FC conditions as a function of the maximum applied field  $H_m$ .

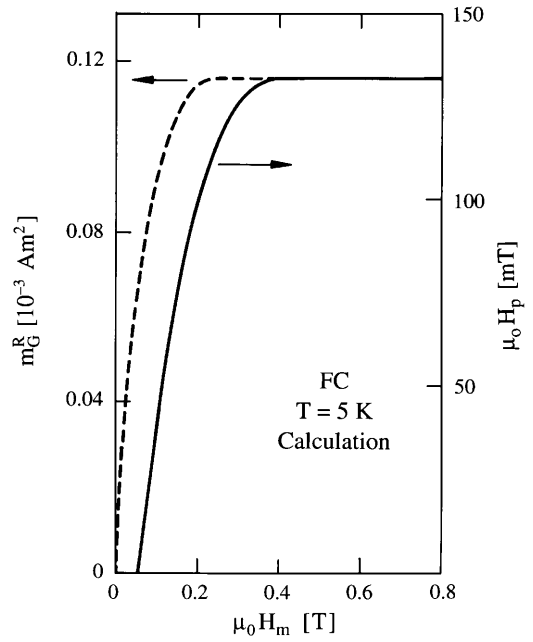


FIG. 16. Calculated intergranular remanent magnetic moment  $m_G^R$  and the measured anomalous peak field  $H_p$  at 5 K under FC conditions as a function of the maximum applied field  $H_m$ .

$m_G^R$ ) and  $H_p$  is caused by the demagnetizing effect of the grains. In the limit  $\Gamma \rightarrow 0$  both  $m_G^R$  and  $H_p$  saturate in the same fashion. Thus, the relative displacement of the curves for  $m_G^R(H_m)$  and  $H_p(H_m)$  is a direct measure of the average demagnetizing factor  $\Gamma$ . Here,  $H_p=0$  at  $H_m=0$  which is different than the full calculations presented in Figs. 14 and 16, indicating that Eq. (17) can only be used when  $H_m \gg H_d$ .

We also have measured  $H_p$  and  $m_G^R$  for  $\mu_0 H_m = 5$  T and found that  $H_p(5 \text{ T}) = H_p(0.8 \text{ T})$  and  $m_G^R(5 \text{ T}) = m_G^R(0.8 \text{ T})$  as expected. It is certainly of interest to investigate the depen-

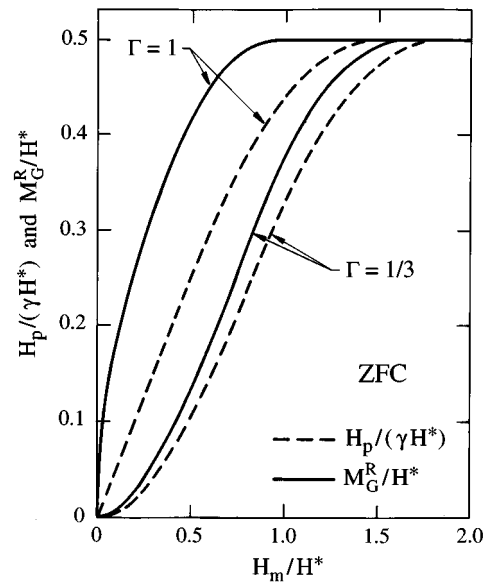


FIG. 17. Calculated values of  $H_p/(\Gamma H^*)$  and  $M_G^R/H^*$  versus  $H_m/H^*$  for two different demagnetizing factors  $\Gamma$  under ZFC conditions using Eqs. (17)–(19).

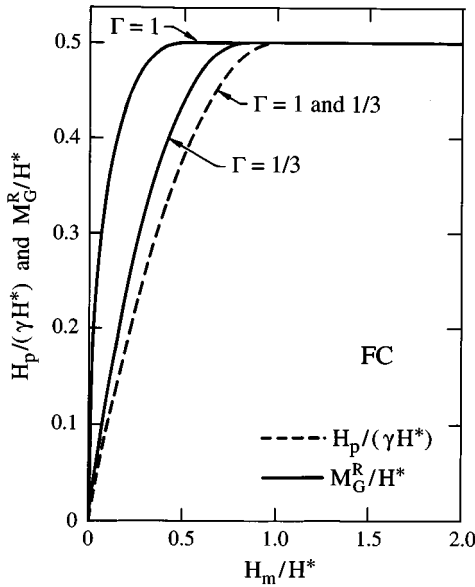


FIG. 18. Calculated values of  $H_p/(\gamma H^*)$  and  $M_G^R/H^*$  versus  $H_m/H^*$  for two different demagnetizing factors  $\Gamma$  under FC conditions using Eqs. (17)–(19).

dence of  $H_p$  and  $m_G^R$  on grain size which has not been done in this paper.

The model, which is described in this paper, reveals that the demagnetizing effect of grains can be used to explain the anomalous peak in the intergranular magnetic moment of PBCCO tapes, caused by the irreversible behavior of the transport current. Besides the grain demagnetization, there seems to be another possible source for the irreversibility of the transport current as discussed by D'yachenko<sup>9</sup> and others. They studied the Josephson current behavior between two superconducting semi-infinite slabs which are in the mixed state with vortex pinning, where the applied field is parallel to the slabs. In the D'yachenko model the Josephson critical current density is

$$J_c^{\text{Jos}} \sim \left| \frac{\sin(\pi\Phi/\Phi_0)}{\pi\Phi/\Phi_0} \right|, \quad (20)$$

where  $\Phi_0$  is the flux quantum and

$$\Phi \approx 4\mu_0 R_G \lambda^2 J_s. \quad (21)$$

Here  $J_s$  is the current density at the surface of a grain at the grain boundary and  $\lambda$  is the London penetration depth of the grains, ignoring the anisotropy of  $\lambda$  ( $\lambda_c \neq \lambda_{ab}$ ). If  $R_G \gg \lambda$  and if the field  $H_a$ , which threads the junction, is large compared to  $R_G J_{cG}$ , one finds

$$J_s \approx J_M \pm J_{cG}, \quad (22)$$

where  $J_M$  is the Meissner shielding current density. The exact expression for  $\Phi$  and  $J_s$  as a function of  $H_a$  and  $H_m$  are given in the Appendix. The  $\pm$  signs in Eq. (22) are for an increasing and decreasing applied field, respectively, and cause the transport current to become irreversible.

In order to find out if the D'yachenko approach can account for our experimental data we have calculated the peak field  $H_p$  for both ZFC and FC conditions from  $\Phi(H_p, H_m) = 0$  where  $\Phi(H_p, H_m)$  is given in the Appendix.

Figure 19 shows for the ZFC case the normalized peak

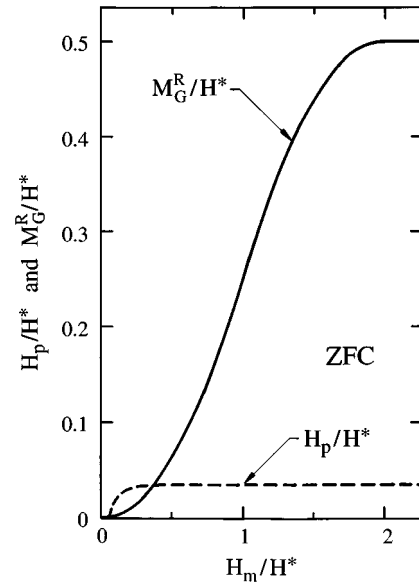


FIG. 19. Calculated normalized anomalous peak field  $H_p/H^*$  in the D'yachenko model and the calculated normalized remanent magnetization  $M_G^R/H^*$  versus the normalized maximum applied field  $H_m/H^*$  under ZFC conditions.

field  $H_p/H^*$  and the normalized remanent intragranular magnetization  $M_G^R/H^*$  as a function of the normalized maximum field  $H_m/H^*$  where  $H^* = J_{cG} R_G$ . Similar results are obtained for the FC case. For the average grain size along the  $a$ - $b$  direction of Bi-2223 grains a value of  $2R_G = 12 \mu\text{m}$  was assumed and  $\lambda = \lambda_{ab} = 0.2 \mu\text{m}$  (Refs. 29 and 30) and  $\mu_0 H_{c1G} = 0.015 \text{ T}$ . According to Fig. 19, independent of  $H^*$ , the D'yachenko model predicts  $H_p(H_m \rightarrow \infty) \ll M_G^R(H_m \rightarrow \infty)$  which is contradictory to the experimental data where  $H_p(H_m \rightarrow \infty) \approx M_G^R(H_m \rightarrow \infty)$ . Figure 19 also demonstrates that the D'yachenko model predicts that  $H_p(H_m)$  saturates at a lower  $H_m$  than the intragranular magnetization  $M_G^R$  which is due to the fact that in the D'yachenko model the Josephson current is only influenced by vortices which are about  $\lambda$  away from the grain boundary and vortices located inside the grains do not affect the Josephson current. The experimental data in Figs. 13 and 15 show that  $M_G^R$  saturates at a lower maximum field  $H_m$  than the peak field  $H_p$  which is in contradiction with the D'yachenko model. Because of these discrepancies, we believe that the origin of the anomalous peak is less due to an irreversible surface current density  $J_s$  but instead mainly due to the demagnetizing effect of the grains. Despite this, the D'yachenko model seems to be suitable to account for the sudden rise of  $J_{cJ}$  often observed in transport current measurements when decreasing the applied field slightly from its maximum value.<sup>9</sup>

## V. CONCLUSIONS

We have measured the magnetic moments of a high-quality PBCCO tape in perpendicular fields up to 1 T at 5 K using a SQUID magnetometer. Subtracting from the total magnetic moment of the intact tape the intragranular magnetic moment of the bent tape, the intergranular magnetic moment, which originates from an induced intergranular



With Eq. (A3) one obtains for  $J_s$ , using Eq. (A5)

$$J_s = \left[ \frac{H_a}{\lambda} - \frac{\Phi_0}{\lambda^2 \mu_0} \int_0^{R_G} d\eta n(\eta) \sinh\left(\frac{\eta - R_G}{\lambda}\right) \right] \tanh\left(\frac{R_G}{\lambda}\right) - \frac{\Phi_0}{\lambda^2 \mu_0} \int_0^{R_G} d\eta n(\eta) \cosh\left(\frac{\eta - R_G}{\lambda}\right). \quad (\text{A6})$$

The Abrikosov vortex distribution,  $n(z)$ , inside the superconducting grains depends on the intragranular critical current density,  $J_{cG}$ . It is assumed that  $J_{cG}$  is independent of the local magnetic induction  $B$  (Bean model). The Abrikosov flux density, when unequal to zero, has the form<sup>26,27</sup>

$$n(z) = n(0) \pm \frac{\mu_0}{\Phi_0} J_{cG} z. \quad (\text{A7})$$

In the following  $B_a$  and  $B_m$  are the inductances at the surface inside the superconductor where  $B_a = \mu_0(H_a + M_{\text{eq}})$  and  $M_{\text{eq}}$  is the equilibrium magnetization. For simplicity we use  $M_{\text{eq}} = -H_a$  for  $0 \leq H_a \leq H_{c1G}$  and  $M_{\text{eq}} = -H_{c1G}$  for  $H_a > H_{c1G}$  where  $H_{c1G}$  is the lower critical field of the grains.

Under ZFC conditions one obtains (i) if  $B_m \leq B^*$   $= \mu_0 J_{cG} R_G$ ,

$$\begin{aligned} \frac{J_s}{J_{cG}} = & \left[ \frac{H_a - B_a / \mu_0}{J_{cG} \lambda} - 2 \sinh\left(\frac{R_G}{\lambda} \frac{B_m - B_a}{2B^*}\right) + \sinh\left(\frac{R_G}{\lambda} \frac{B_m}{B^*}\right) \right] \\ & \times \tanh\left(\frac{R_G}{\lambda}\right) - 1 + 2 \cosh\left(\frac{R_G}{\lambda} \frac{B_m - B_a}{2B^*}\right) \\ & - \cosh\left(\frac{R_G}{\lambda} \frac{B_m}{B^*}\right), \end{aligned} \quad (\text{A8})$$

(ii) if  $B_m > B^*$  and  $B_m - 2B^* \leq B_a \leq B_m$ ,

$$\begin{aligned} \frac{J_s}{J_{cG}} = & \left[ \frac{H_a - B_a / \mu_0}{J_{cG} \lambda} - 2 \sinh\left(\frac{R_G}{\lambda} \frac{B_m - B_a}{2B^*}\right) + \sinh\left(\frac{R_G}{\lambda}\right) \right] \\ & \times \tanh\left(\frac{R_G}{\lambda}\right) - 1 + 2 \cosh\left(\frac{R_G}{\lambda} \frac{B_m - B_a}{2B^*}\right) - \cosh\left(\frac{R_G}{\lambda}\right), \end{aligned} \quad (\text{A9})$$

and (iii) if  $B_m > B^*$  and  $-B_m \leq B_a \leq B_m - 2B^*$ ,

$$\frac{J_s}{J_{cG}} = \frac{H_a - B_a / \mu_0}{J_{cG} \lambda} \tanh\left(\frac{R_G}{\lambda}\right) - 1 + \frac{1}{\cosh(R_G / \lambda)}. \quad (\text{A10})$$

It is interesting to note that  $J_s$  in Eq. (A10) is independent of  $B_m$  and that one obtains from Eq. (A10) for  $B_a = 0$  and  $R_G \gg \lambda$  the result  $H_p = (\lambda / R_G) H^*$ .

Under FC conditions one obtains (i) if  $B_m \leq B^*/2$ ,

$$\begin{aligned} \frac{J_s}{J_{cG}} = & \left[ \frac{H_a - B_a / \mu_0}{J_{cG} \lambda} + \frac{B_m}{\mu_0 J_{cG} \lambda} \cosh\left(\frac{R_G}{\lambda}\right) \right. \\ & \left. - \sinh\left(\frac{R_G}{\lambda} \frac{B_m - B_a}{B^*}\right) \right] \tanh\left(\frac{R_G}{\lambda}\right) - 1 \\ & - \frac{B_m}{\mu_0 J_{cG} \lambda} \sinh\left(\frac{R_G}{\lambda}\right) + \cosh\left(\frac{R_G}{\lambda} \frac{B_m - B_a}{B^*}\right) \end{aligned} \quad (\text{A11})$$

(ii) if  $B_m > B^*/2$  and  $B_m - B^* \leq B_a \leq B_m$  one obtains Eq. (A11) and if  $-B_m \leq B_a < B_m - B^*$  one obtains Eq. (A10) as the magnetic field profiles for ZFC and FC become identical.

Because  $J_s$  is independent of  $y$  in the slab approximation, one obtains from Eq. (A2)

$$\varphi(y) = \frac{4\pi\mu_0}{\Phi_0} [(\xi + t/2)H_a + \lambda^2 J_s] y + \varphi_0. \quad (\text{A12})$$

The critical Josephson current density,  $J_c^{\text{Jos}}$ , is given by determining the constant  $\varphi_0$  which maximizes the current density,  $J^{\text{GB}}$ , across a grain-boundary junction of width  $2R_G$  where

$$\begin{aligned} J^{\text{GB}} = & \frac{J_0}{2R_G} \int_{-R_G}^{R_G} \sin\{4\pi\mu_0 [(\xi + t/2)H_a + \lambda^2 J_s] y / \Phi_0 \\ & + \varphi_0\} dy. \end{aligned} \quad (\text{A13})$$

$J_0$  is the Josephson current density if no flux is trapped inside grains and no field is applied. One finds

$$J_c^{\text{Jos}} = J_0 \left| \frac{\sin(\pi\Phi/\Phi_0)}{\pi\Phi/\Phi_0} \right|, \quad (\text{A14})$$

where

$$\Phi(H_a, H_m) = 4\mu_0 R_G [(\xi + t/2)H_a + \lambda^2 J_s(H_a, H_m)]. \quad (\text{A15})$$

According to Eq. (A14), the critical Josephson current density  $J_c^{\text{Jos}}$  peaks at a field  $H_p$  for which

$$\Phi(H_p, H_m) = 0. \quad (\text{A16})$$

Because  $\lambda \gg \xi + t/2$ , one can obtain  $H_p$  also from  $J_s(H_p, H_m) = 0$ .

<sup>1</sup>L. N. Bulaevskii, L. L. Daemen, M. P. Maley, and J. Y. Coulter, Phys. Rev. B **48**, 13 798 (1993).

<sup>2</sup>K.-H. Müller, C. Andrikidis, H. K. Liu, and S. X. Dou, Phys. Rev. B **50**, 10 218 (1994).

<sup>3</sup>J. R. Clem, Physica C **153–155**, 50 (1988).

<sup>4</sup>J. E. Evetts and B. A. Glowacki, Cryogenics **28**, 641 (1988).

<sup>5</sup>M. E. McHenry, M. P. Maley, and J. O. Willis, Phys. Rev. B **40**, 2666 (1989).

<sup>6</sup>A. A. Zhukov, D. A. Komarkov, G. Karapetrov, S. N. Gordeev,

and R. I. Antonov, Supercond. Sci. Technol. **5**, 338 (1992).

<sup>7</sup>K.-H. Müller and D. N. Matthews, Physica C **206**, 275 (1993).

<sup>8</sup>E. Altshuler, J. Musa, J. Barroso, A. R. R. Papa, and V. Venegas, Cryogenics **33**, 308 (1993).

<sup>9</sup>A. I. D'yachenko, Physica C **213**, 167 (1993).

<sup>10</sup>K. Sato, T. Hikata, H. Mukai, M. Ueyama, N. Shibuta, T. Kato, T. Masuda, M. Nagata, K. Iwata, and T. Mitsui, IEEE Trans. Magn. **MAG-27**, 1231 (1991).

<sup>11</sup>R. L. Peterson and J. W. Ekin, Phys. Rev. B **37**, 9848 (1988).

- <sup>12</sup>K. Kwasnitza and St. Clerc, *Adv. Cryog. Eng.* **40**, 53 (1994).
- <sup>13</sup>K.-H. Müller, C. Andrikidis, H. K. Liu, and S. X. Dou, *Physica C* **235–240**, 3037 (1994).
- <sup>14</sup>M. R. Cimberle, C. Ferdeghini, R. Flükiger, E. Giannini, G. Grasso, D. Marrè, M. Putti, and A. S. Siri, *Physica C* **251**, 61 (1995).
- <sup>15</sup>H. K. Liu, Y. C. Guo, and S. X. Dou, *Supercond. Sci. Technol.* **5**, 591 (1992).
- <sup>16</sup>J. R. Clem, *Phys. Rev. B* **43**, 7837 (1991).
- <sup>17</sup>A. Majhofer, T. Wolf, and W. Dieterich, *Phys. Rev. B* **44**, 9634 (1991).
- <sup>18</sup>T. Wolf and A. Majhofer, *Phys. Rev. B* **47**, 5383 (1993).
- <sup>19</sup>M. Tinkham and C. J. Lobb, in *Solid State Physics: Advances in Research and Applications*, edited by H. Ehrenreich and D. Turnbull (Academic, New York, 1989), Vol. 42, p. 91.
- <sup>20</sup>E. H. Brandt and M. Indenbom, *Phys. Rev. B* **48**, 12 893 (1993).
- <sup>21</sup>F. Zeldov, J. R. Clem, M. McElfresh, and M. Darwin, *Phys. Rev. B* **49**, 9802 (1994).
- <sup>22</sup>E. C. Stoner, *Philos. Mag.* **36**, 803 (1945).
- <sup>23</sup>G. Waysand, *Europhys. Lett.* **5**, 73 (1988).
- <sup>24</sup>M. L. Hodgdon, R. Navarro, and L. J. Campbell, *Europhys. Lett.* **16**, 677 (1991).
- <sup>25</sup>A. Barone and G. Paterno, *Physics and Applications of the Josephson Effect* (Wiley, New York, 1982).
- <sup>26</sup>C. P. Bean, *Phys. Rev. Lett.* **8**, 250 (1962).
- <sup>27</sup>C. P. Bean, *Rev. Mod. Phys.* **36**, 31 (1964).
- <sup>28</sup>J. R. Clem and Z. Hao, *Phys. Rev. B* **48**, 13 774 (1993).
- <sup>29</sup>J. R. Cooper, L. Forró, and B. Keszei, *Nature (London)* **343**, 444 (1990).
- <sup>30</sup>A. Schilling, F. Hulliger, and H. R. Ott, *Z. Phys. B* **82**, 9 (1991).
- <sup>31</sup>A. V. Nikulov and D. Yu. Remisov, *Supercond. Sci. Technol.* **4**, 312 (1991).
- <sup>32</sup>L. N. Bulaevskii, J. R. Clem, L. I. Glazman, and A. P. Malozemoff, *Phys. Rev. B* **45**, 2545 (1992).